Advances in Science and Technology Research Journal

Advances in Science and Technology Research Journal, 2027, 21(1), 86–102
https://doi.org/10.12913/22998624/231183
ISSN 2299-8624, License CC-BY 4.0

Received: 2026.07.17
Accepted: 2026.11.15
Published: 2026.12.01

Proof-of-concept evaluation of the Teager-Kaiser energy operator for condition assessment of water-lubricated plain bearings in mining pump applications

Jędrzej Blaut[1], Marta Drosińska-Komor[2], Jakub Wróbel[3], Beata Borska[4], Antoni Lis[5], Piotr Blaut[6], Łukasz Breńkacz[7*]

[1] Faculty of Mechanical Engineering and Robotics, AGH University of Krakow, ul. Mickiewicza 30, 30-059 Krakow, Poland
[2] Faculty of Mechanical Engineering and Ship Technology, Gdańsk University of Technology, ul. Narutowicza 11/12, 80-233 Gdańsk, Poland
[3] Faculty of Mechanical Engineering, Wroclaw University of Science and Technology, ul. Łukasiewicza 7/9, 50-371 Wroclaw, Poland
[4] KWK Ruda, ul. Kłodnicka 54, 41-706 Ruda Śląska, Poland
[5] Elmodis Sp. z o.o., Aleja Pokoju 1, 31-548 Kraków, Poland
[6] Institute of Physical Chemistry, Polish Academy of Sciences, ul. Marcina Kasprzaka 44/52, 01-224 Warsaw, Poland
[7] Institute of Fluid-Flow Machinery, Polish Academy of Sciences, Fiszera 14, 80-231 Gdańsk, Poland
* Corresponding author's e-mail: lukasz.brenkacz@imp.gda.pl

ABSTRACT

Reliable condition monitoring is needed for water-handling machinery used in mining, where abrasive media, humidity, and variable loading can accelerate pump and bearing degradation. This study investigated the Teager-Kaiser energy operator (TKEO) as a complementary diagnostic tool for pump-bearing vibration analysis, with emphasis on water-lubricated plain bearings used in mining applications. Four synthetic signal models—normal operation, unbalance, localised surface defects, and hydrodynamic instability—were analysed using time-domain statistics, Fast Fourier Transform (FFT) spectra, and the three-sample discrete TKEO. A controlled laboratory proof-of-concept complemented the simulations by comparing displacement and acceleration records from three imposed bearing configurations (A–C) at a constant shaft speed of 25 Hz. The configurations were produced by rotating the bearing and thereby changing the location of the lubrication gap; they were not independently validated as stable, transient, or unstable dynamic states. Conventional RMS and FFT measures captured overall vibration levels and rotational harmonics. The TKEO-derived indicators also changed across the imposed configurations, but their numerical ratios are not directly comparable with conventional RMS because the two quantities have different amplitude scaling. Accordingly, the observed configuration-dependent changes are reported as descriptive proof-of-concept results and do not establish greater diagnostic sensitivity, statistical superiority, classification performance, or field validity. The specific contribution of this proof-of-concept is an application-focused comparison of conventional and TKEO-derived descriptors for displacement and acceleration records from a water-lubricated plain bearing under imposed Configurations A–C. The four synthetic signals were used only to illustrate the response of the processing methods to selected signal constructions and were not treated as validation or physical counterparts of the experimental configurations.

Keywords: water-lubricated plain bearing, centrifugal pump, mining machinery diagnostics, vibration signal processing, Teager-Kaiser energy operator.

INTRODUCTION

Centrifugal pumps are central to mine dewatering, hydrotransport, and process-water systems. Their rotating and stationary components are exposed to unbalance, alignment errors, bearing degradation, hydraulic disturbances and abrasive media. Therefore, monitoring combines vibration and operating variables such as pressure, flow, temperature, speed, and, for motor-driven units, electrical quantities. The practical objective was to recognise changes early enough to plan maintenance without overstating what a single indicator can prove.

The synchronous response produced by rotor unbalance also reflects the dynamic properties of the rotor–support system; measured responses have been used to identify bearing-support stiffness and damping [1]. Hydrodynamic disturbances generate broadband components and discrete spectral peaks that can support pump-condition assessment [2].

Mining pumps must maintain drainage capacity under high humidity, fluctuating loads, and contaminated water. Pumping can account for a substantial share of mine energy use [3]. Fault detection is consequently relevant to both availability and operating cost. Model-based and data-driven diagnostic concepts can improve equipment availability [4]. Intelligent monitoring and control have also been proposed as a route to lower pumping energy use [5].

Research on rotating machinery supports combining physical rotor-dynamic knowledge with signal processing. A vibration-based system for an ORC microturbine used numerical analysis to choose monitoring points and interpret rotational components [6]. A genetic-algorithm approach showed how interacting turbine degradations can be separated computationally [7].

Previous studies by the authors investigated TKEO under controlled laboratory conditions and generic hydrodynamic bearing models [10]. A related study examined dispersion entropy as an additional signal-processing measure [8, 9]. The present work narrowed that line of research to a water-lubricated plain bearing and experimentally imposed changes among three bearing configurations, designated A–C. Reliable monitoring of rotating equipment is particularly important in mining [11], while vibration measurements have also been related to pump hydraulic performance and impeller damage [12].

Earlier studies by the authors addressed related but distinct questions. Reference [10] applied TKEO to rotor-unbalance assessment in a system supported by hydrodynamic plain bearings. Reference [9] applied dispersion entropy to displacement records and rotational trajectories from a water-lubricated plain-bearing test rig, while Reference [8] examined the influence of sliding-window length on dispersion-entropy analysis. The present study did not claim the first application of TKEO to hydrodynamic bearings or the first use of a water-lubricated bearing test rig. Its narrower contribution is the joint, descriptive assessment of conventional RMS, selected FFT components, and three-sample TKEO descriptors for displacement and acceleration records from imposed bearing Configurations A–C at a fixed shaft speed, accompanied by illustrative synthetic signal models.

Operational context of mining pumps and water-lubricated bearings

Mining machinery diagnostics must respond to increasing depth and operational complexity [13]. Higher ambient temperatures can reduce reliability and increase the need for inspection [14]. Energy- and resource-efficient mechanisation is also pursued in other mining transport systems [15].

Water-lubricated bearings offer low friction, cooling, and reduced environmental burden [16]. Their corrosion resistance and lubrication characteristics support applications where oil contamination is undesirable [17]. In mining pumps, their condition affects the reliability of the complete rotor–pump system [18]. Experiments on hydrodynamic journal bearings show that stiffness and damping can be identified from measured responses [19]. These coefficients may vary substantially near resonance and hydrodynamic instability [20], which complicates the interpretation of any energy-based indicator.

Mine pumps operate with corrosion, abrasion, and solids, so materials and well or system geometry must be selected carefully [21]. Chemically aggressive and particle-laden media accelerate component degradation [22]. Solids can erode the impeller and casing and reduce pump efficiency [23]. Slurry-pump wear depends on particle concentration [24] and particle shape [25]. Particle size and hardness are additional influential factors [26]. Housing investigations have documented cutting, tearing, and deformation mechanisms [27].

Material selection and protective design are, therefore, part of the diagnostic context. Metallic alloys have been compared for erosion resistance [28], and neural-network methods have been applied to material-performance assessment [29]. Replaceable elastomeric or alloy liners are used in abrasive slurry pumps [30]. Excessive pressure, overload, dry running, and thermal changes can damage bearings or degrade lubrication [31], while installation errors, poor pump selection, and mine humidity or dust add further uncertainty [32].

Research gap, aim, and contributions

Most published pump-diagnostic studies focused either on conventional spectral indicators, generic bearing models, or steady operating conditions. The present work addressed a narrower question: whether conventional and TKEO-derived indicators exhibit configuration-dependent changes among three imposed bearing configurations (A–C) at a fixed shaft speed. The contribution is threefold. First, four synthetic signals represent normal operation, unbalance, bearing-surface damage, and hydrodynamic instability. Second, a controlled test rig provides displacement and acceleration records for Configurations A–C. Third, the same time-domain, frequency-domain, and TKEO measures were used to describe the simulated responses and the configuration-dependent experimental trends. The experimental component was intentionally treated as a proof-of-concept; it did not provide independent physical validation of dynamic-state labels, statistical classification performance, or direct validation in an underground mine.

Accordingly, the aim was to evaluate configuration-dependent TKEO responses and their complementarity with conventional RMS and FFT measures. The work used the retained simulation outputs and laboratory records without claiming independently validated dynamic states or a statistically validated industrial classifier. The working hypothesis (H1) is that, for the retained records obtained from imposed bearing Configurations A–C at a constant shaft speed of 25 Hz, conventional and TKEO-derived indicators will exhibit observable configuration-dependent changes and provide complementary signal descriptions. H1 does not assume that TKEO is diagnostically superior, the configurations are independently validated physical states, or the indicators provide a statistically validated classifier. Accordingly, the contribution is methodological and application-specific, rather than a claim of a new diagnostic classifier. The study applied the same descriptive analysis framework to displacement and acceleration records from a water-lubricated plain bearing and explicitly separates the experimental comparison from four synthetic demonstrations of operator behaviour.

MATERIALS AND METHODS

Teager-Kaiser energy operator and diagnostic indicators

The Teager-Kaiser energy operator (TKEO) is a nonlinear operator used to estimate the instantaneous energy of a signal. It was developed by Hubert M. Teager and Shushan M. Teager and subsequently described by J. F. Kaiser in "On a simple algorithm to calculate the 'energy' of a signal". TKEO is commonly applied to non-stationary signals, including speech, biological signals (ECG and EMG), and mechanical vibration signals used in bearing diagnostics [33–35]. The operator responds to rapid joint changes in signal amplitude and frequency.

The energy operator is defined in the continuous form [10]:

$$\psi[x(t)] = \dot{x}^2(t) - x(t)\ddot{x}(t) \tag{1}$$

where: $x(t)$ – displacement, $\dot{x}(t)$ – first time derivative of displacement, $\ddot{x}(t)$ – second time derivative of displacement.

For the sampled signals, the discrete operator was evaluated as

$$\psi[x(n)] = x^2(n) - x(n-1)x(n+1).$$

Because the expression requires adjacent samples, the first and last samples were excluded from the derived TKEO sequence. The reported TKEO amplitude is the peak-to-peak range of that sequence, and RMS(TKEO) is its root-mean-square value. TKEO results are reported in arbitrary units [a.u.] because a unique physical energy unit cannot be assigned across displacement and acceleration inputs.

The operator uses only three adjacent signal samples and is therefore computationally simple. This short local support enables rapid analysis of changes in the signal-derived energy measure.

TKEO is relevant to pump diagnostics because it responds to rapid changes in non-stationary signals. Due to its low computational complexity, this method is suitable for online implementation in dynamic monitoring systems. The signal features of diagnostic interest encompass various operational phenomena, such as bearing wear, which typically manifests as characteristic pulse signals. Additionally, cavitation generates impulsive signal components resulting from bubble formation and collapse, whereas shaft unbalance induces time-varying oscillations. Finally, rotor-to-housing friction produces short impulsive signal components that can be effectively detected. Table 1 summarises the principal advantages and limitations of using TKEO for pump diagnostics.

Simulation signal models

The simulation study was designed to illustrate how the time-domain, FFT, and TKEO representations respond to four predefined signal constructions: a fundamental harmonic, increased synchronous amplitude with harmonics, added Gaussian pulses, and amplitude-modulated Gaussian noise. These models are not assigned to experimental Configurations A, B, or C. In particular, the synthetic hydrodynamic-instability model is not used to validate Configuration C or to identify a physical instability in the experiment.

One of the key issues examined in the simulation studies was rotor unbalance, a common problem in pump systems. Unbalance can result from assembly errors, wear of rotating parts, or asymmetric rotor loading. It is characterised by a vibration signal at a frequency corresponding to the machine speed, often with increased amplitude, resulting in pulsations along the radial axis.

Interpreting the measured response becomes more complex when rotor flexibility and residual unbalance are considered. Xu et al. proposed an identification approach that used two independent sets of the unbalance-response data to estimate bearing stiffness and damping in a flexible rotor system in the presence of unknown residual unbalances. Their numerical and experimental results showed that isolating the contribution of residual unbalance from the response associated with the investigated bearing parameters is important for obtaining reliable estimates of the system dynamics [36]. Although the model adopted in the present proof-of-concept study represents unbalance using a simplified harmonic signal, future extensions should account for rotor flexibility, speed-dependent bearing properties, residual unbalance, and the possible interaction between unbalance excitation and hydrodynamic instability.

Rotor unbalance is important not only as a diagnostic symptom but also as a potential target for automatic corrective action. Breńkacz et al. analysed a continuously adjustable correction-mass system using a numerical model of a 5 MW offshore wind turbine and demonstrated that redistributing the correction mass can reduce unbalance-induced vibration and associated fatigue effects [37]. Although the present study concerned fault detection in a centrifugal pump rather than active balancing, the results underscore the importance of identifying the synchronous rotational component and distinguishing it from broadband or impulsive signatures associated with hydrodynamic instability, cavitation, or local bearing-surface damage.

The baseline harmonic signal represented normal operation:

$$x_N(t) = A_0 \sin(2\pi f_r t + \varphi_0) \qquad (2)$$

where: $A_0 = 0.15$ mm, $f_r = 25$ Hz, and $\varphi_0 = \frac{\pi}{4}$

Rotor-unbalance signal model

Rotor unbalance was represented by three harmonics of the rotational frequency, with harmonic amplitudes decreasing in proportion to 1/n:

Table 1. Advantages and disadvantages of using TKEO for pump diagnostics

Advantages	Disadvantages
Early fault localisation	Sensitivity to noise can lead to falsification of results
Computational simplicity	Difficulty in interpreting results
Pulse sensitivity	Use of additional filters for signal analysis
No need to know signal parameters	Lack of versatility
Detection of non-stationary signals	–

$$x_U(t) = kA_0 \sum_{n=1}^{3} \frac{\sin(2\pi n f_r t + \varphi_n)}{n} \quad (3)$$

where: k = 2 and the three phases φ_n were sampled independently from $U(0,2\pi)$. The harmonic amplitudes were $\frac{kA_0}{n}$ for n = 1, 2, and 3, giving a fundamental amplitude of 0.30 mm.

Bearing-surface-damage signal model (scratches or chipping)

Bearing-surface damage was represented by adding 10 randomly located Gaussian impulses to the baseline harmonic:

$$x_D(t) = x_N(t) + \\ + \sum_{i=1}^{10} \frac{1}{3} \exp\left[\frac{-(t - t_i)^2}{2\sigma^2}\right] \quad (4)$$

where: each impulse centre t_i was sampled independently from $U(0,2.0\text{ s})$, $\sigma = 0.11$ s, and the peak coefficient $\frac{1}{3}$ is expressed in the same displacement units as the simulated signal. This coefficient is a mathematical signal-model parameter and is not interpreted as a physical defect amplitude.

Hydrodynamic-instability signal model (lubricating-film fluctuations)

The hydrodynamic-instability case was represented by Gaussian-white-noise modulation of the harmonic amplitude:

$$x_H(t) = [A_0 + \alpha(t)] \sin(2\pi f_r t + \varphi_0) \quad (5)$$

where: $\alpha(t)$ is a Gaussian white-noise sequence with mean 0, standard deviation 0.2, and variance 0.04.

All four synthetic signals were generated at a sampling frequency of 12,800 Hz over 2.0 s, giving 25,600 samples per signal, and one realisation was generated for each model. The common baseline parameters were f_r = 25 Hz, A_0 = 0.15 mm, and $\varphi_0 = \frac{\pi}{4}$. No fixed pseudorandom-generator seed was set or retained for the random harmonic phases, impulse locations, or Gaussian-noise sequence. Consequently, the documented distributions and deterministic parameters can be reproduced, but the precise stochastic waveforms shown in the figures cannot be regenerated on a sample-by-sample basis. A single realisation per model does not characterise realisation-to-realisation variability. The models are illustrative mathematical signal constructions; they are not physical models of the bearing or lubricating film and do not validate or map one-to-one onto experimental Configurations A–C.

The simulation and experiment, therefore, address different questions. The simulations illustrate method response under controlled signal constructions, whereas the experimental records provide a descriptive comparison of the imposed bearing Configurations A–C. No one-to-one correspondence between the four simulated cases and the three experimental configurations was assumed.

Experimental test rig and imposed configurations

To analyse the dynamic behaviour of a water-lubricated plain bearing, a test rig (shown in Figure 1) was designed and built. The experiment was conducted under controlled conditions and serves as a proof-of-concept to demonstrate the applicability of the proposed signal processing approach.

The numbering 1–10 shown in Figure 1 is retained. The corresponding elements are: (1) 3.5 kW drive motor; (2) coupling; (3) laser tachometer; (4) bearing support; (5) 20 mm-diameter shaft; (6) MDS10PO eddy-current displacement system; (7) dial-gauge displacement sensor; (8) PCB-356B08 triaxial accelerometer; (9) tested bearing; and (10) bearing/loading assembly. The tachometer covered 2.5–99,999 rpm at a measurement distance of 50–500 mm. The eddy-current system had a sensitivity of 8 V/mm and a 2–4 mm measuring range. The accelerometer had a sensitivity of 10 mV/(m/s²), a ±490 m/s² measuring range, and a 0.5–5000 Hz frequency range. A 1 mm shaft deflection generated an estimated load of approximately 80 N; deflection was checked with the dial gauge at 0.02 mm resolution.

A constant shaft speed of 25 Hz was used during the tests, reflecting a controlled operating scenario selected for qualitative assessment rather than parametric exploration across multiple operating regimes. The bearing was rotated to change the location of the lubrication gap, producing three imposed test configurations

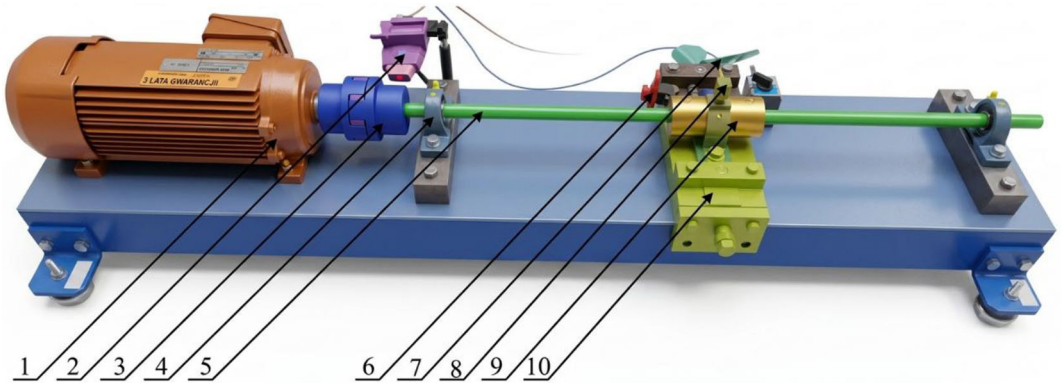


Figure 1. Laboratory test rig used to impose bearing Configurations A–C. Adapted from Blaut [9] The numbering 1–10 within the graphic is retained, and the corresponding element descriptions are provided in the text

designated A, B, and C. For traceability, Configuration A corresponds to the record previously labelled "stable", Configuration B to "transient", and Configuration C to "unstable". These designations identify the imposed bearing orientations and lubrication-gap locations only. No independent physical criterion – such as shaft-centre orbits, waterfall spectra, subsynchronous components, Sommerfeld number, eccentricity ratio, measured load or gap position, or direct evidence of water whirl – was available to validate the configurations as stable, transient, or unstable dynamic states. The experimental records are therefore used only for a qualitative comparison of signal-processing indicators across the three imposed configurations.

Water was supplied by gravity from a reservoir positioned approximately 0.10 m above the tested bearing. The water passed freely through the bearing and discharged to drain; no forced-pressure supply was used. Volumetric flow rate and supply pressure were not measured. Accordingly, the supply condition is reported as an approximately 0.10 m hydrostatic head, rather than as a measured pressure. Water temperature was not instrumentally recorded; ambient and water temperatures during the tests were approximately 20–22 °C. No more precise flow rate, pressure, or temperature value is inferred.

Signal acquisition and processing

Displacement and acceleration channels in the X and Y directions were acquired at the tested-bearing assembly at a sampling frequency of 12,800 Hz for approximately 10 s for each acquisition. Four independent repeats were acquired for each analysed configuration as part of a broader experimental campaign comprising 175 measurements overall. The first 1.0 s of each acquisition, comprising 12,800 samples, was selected for processing. The signals were low-pass filtered using a fourth-order Butterworth filter with a cutoff frequency of 100 Hz. No demeaning or detrending was applied. This description preserves traceability to the processing used for the reported results and should not be interpreted as a recommendation to retain the static component when estimating vibration-only displacement RMS. FFT spectra were calculated from the selected 1.0-s segments using a rectangular window with no additional taper, 0% overlap, and a frequency resolution of 1 Hz; the spectral range was 0–6400 Hz. The subsequent processing sequence comprised calculation of the time-domain mean, peak-to-peak amplitude, and RMS, FFT amplitudes at 25, 50, and 75 Hz, application of the three-sample discrete TKEO, as well as calculation of TKEO amplitude and RMS. No amplitude-normalisation step was documented for the experimental TKEO calculation, and none was claimed. Absolute TKEO magnitudes from displacement and acceleration channels were therefore not treated as directly comparable physical quantities; the reported observations were restricted to descriptive within-channel changes among Configurations A–C. The tested bearing was a water-lubricated plain bearing with a rubber lining. Its length was 80 mm, it contained eight lubrication grooves/channels, and the tested shaft diameter was 20 mm. The retained documentation does not provide the

radial or diametral clearance, a separate bearing bore or outer diameter, or the dimensions of the individual grooves/channels; therefore, these values are not reconstructed. Configurations A–C describe the controlled change produced by rotating the bearing and changing the lubrication-gap location at a constant shaft speed of 25 Hz; they are not treated as independently confirmed dynamic states.

The FFT spectra shown for the four synthetic signals in Figure 2 were generated separately using a Hann (Hanning) window. The plotted FFT quantity is the unscaled magnitude, calculated as the modulus of the FFT using np.abs(fft_signal), without amplitude normalisation. Consequently, the displayed synthetic FFT values must not be interpreted as physical signal amplitudes in millimetres. This processing applies only to the synthetic Figure 2 spectra and does not describe the FFT processing of the experimental records.

RESULTS

Simulation results

The following simulation results show the qualitative response of the three processing domains to the four predefined signal constructions. They do not predict, classify, or validate experimental Configurations A–C, and no simulated case is treated as the physical counterpart of an experimental record.

The normal-operation signal model is characterised by a stable harmonic signal with an amplitude of 0.15 mm at a fundamental frequency of 25 Hz. FFT analysis shows a single, distinct peak at the fundamental frequency, while the TKEO operator produces a stable, low-noise energy waveform. This is illustrated in Figure 2. Rotor unbalance manifests as increased vibration amplitude (0.30 mm) and additional harmonics in the FFT spectrum. A characteristic feature is the presence of up to three harmonics, with the fundamental

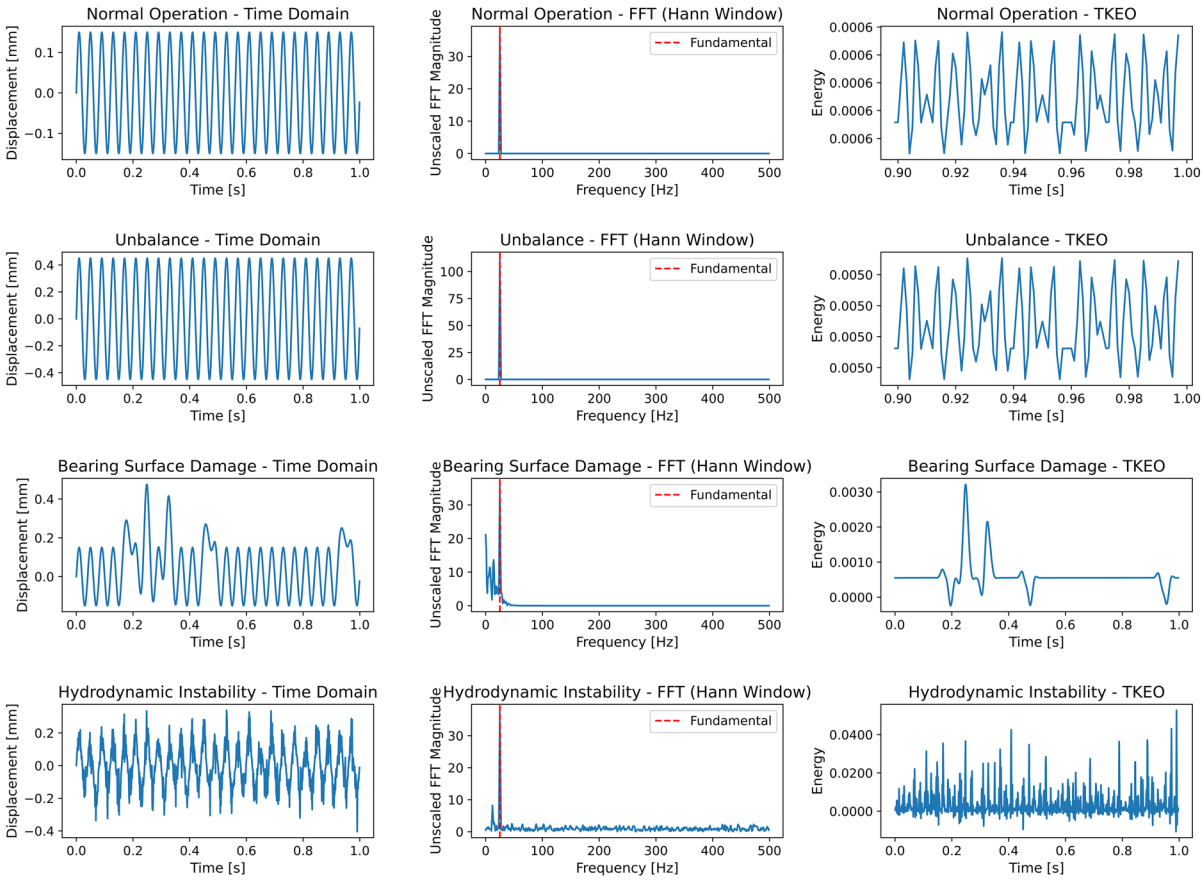


Figure 2. Vibration signal characteristics for the four modelled cases using time-domain, FFT, and TKEO methods. The synthetic FFT spectra were generated using a Hann window and display the unscaled FFT magnitude without amplitude normalisation; these values must not be read as physical signal amplitudes in millimetres. These settings apply only to the synthetic spectra and not to the experimental records. Axis limits and displayed time intervals differ among panels and must be read from each displayed axis

frequency remaining dominant. TKEO analysis shows increased energy levels compared to normal operating conditions. Gaussian pulses characterise the bearing-surface-damage signal construction in the time signal. The FFT spectrum shows energy dissipation over a wider frequency band, while the TKEO operator reveals sharp energy peaks corresponding to the pulses. In the hydrodynamic-instability illustration, hydrodynamic instability manifests as increased noise levels while maintaining the nominal amplitude (0.15 mm). In the FFT analysis, a broadened frequency band is observed, while the TKEO operator reveals irregular energy fluctuations characteristic of lubricating-film disturbances.

The analysis showed that combining the three diagnostic methods differentiates the four modelled operating cases qualitatively. Particularly important is the complementarity of the methods used, as each method highlights different aspects of the diagnostic signals under study.

Table 2 lists the parameters characterising the four illustrative synthetic signal cases of the plain bearing pump. Each state is described by five basic parameters: signal type, vibration amplitude, fundamental frequency, presence of harmonics, and noise level.

Table 2 summarises the four modelled cases. Normal operation uses 0.15 mm at 25 Hz without added harmonics or pulses and with low noise. Unbalance increases the amplitude to 0.30 mm and includes up to three harmonics. Bearing-surface damage retains the nominal 0.15 mm amplitude and adds Gaussian pulses. Hydrodynamic instability also retains 0.15 mm, but uses a high noise level. These parameter combinations define the synthetic comparison; they are not trained classifier thresholds.

Therefore, the simulations demonstrate differences in method response to selected mathematical signal features only. Their agreement with an expected qualitative pattern is not evidence that the experimental configurations represent the corresponding simulated fault or instability cases.

Experimental results

The record for Configuration A is characterised by relatively low amplitude and RMS values in both displacement and acceleration. Its frequency spectrum contains components at 25, 50, and 75 Hz, and the TKEO sequence has relatively small amplitude and RMS values. These observations describe the retained record for Configuration A and do not independently establish a physically stable bearing state. These characteristics are illustrated in Figure 3 and Table 3.

Relative to Configuration A, the retained record for Configuration B shows moderate increases in amplitude and RMS, particularly in the displacement signals. Higher amplitudes are also visible at selected harmonic components, and the TKEO indicators increase. These observations describe the differences between the imposed configurations and are not interpreted as confirmation of a transient dynamic state. These characteristics are illustrated in Figure 4 and Table 4.

The retained record for Configuration C shows higher displacement and acceleration amplitudes and RMS values than Configurations A and B. Larger components are also visible at 25, 50, and 75 Hz, and the TKEO amplitude and RMS increase. These signal differences are not, by themselves, evidence of a physically unstable state or confirmed hydrodynamic instability. These characteristics are illustrated in Figure 5 and Table 5.

Table 6 provides a qualitative comparison of the role, retained-record observations, and principal limitations of RMS, FFT, and TKEO in the present study.

This qualitative comparison does not rank diagnostic sensitivity or establish the superiority of any method.

Across the acceleration channels, both the conventional time-domain RMS and RMS(TKEO) changed among the retained records for Configurations A, B, and C. From Configuration A to B, RMS(TKEO) increased by factors of 2.46 in X

Table 2. Parameterisation of the four illustrative synthetic signal cases

Signal Type	Amplitude [mm]	Fundamental frequency [Hz]	Additional harmonics	Impulses	Noise level
Normal operation	0.15	25	No	No	Low
Unbalance	0.30	25	Yes (up to 3)	No	Low
Bearing surface damage	0.15	25	No	Yes (Gaussian)	Low
Hydrodynamic instability	0.15	25	No	No	High

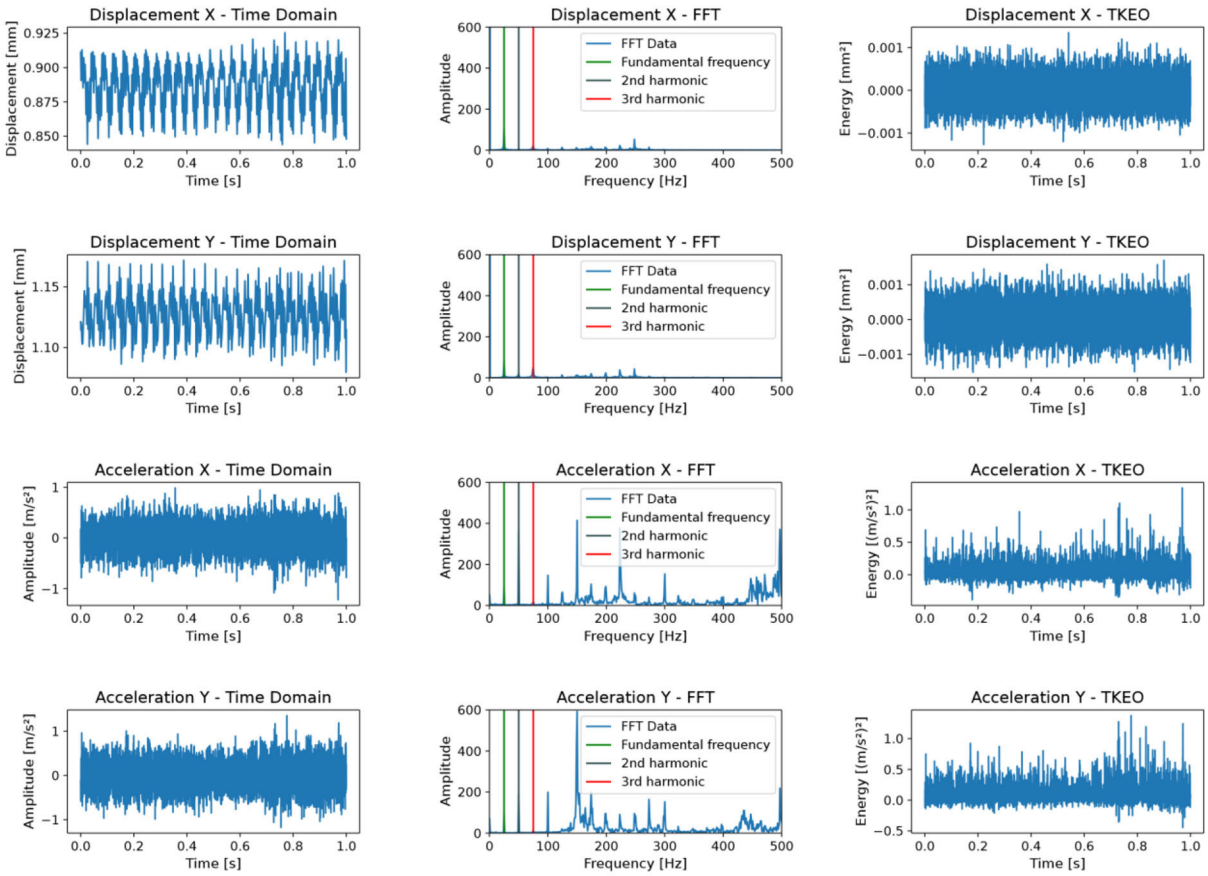


Figure 3. Vibration signal characteristics for the single retained record from the imposed bearing Configuration A, analysed using time-domain, FFT, and TKEO methods. Axis limits differ across panels and configurations and must be read from each displayed axis

Table 3. Descriptive parameters from the single retained displacement and acceleration record for the imposed bearing Configuration A

Channel	Mean (Time)	Amplitude (Time)	RMS (Time)	FFT Amp @25Hz	FFT Amp @50Hz	FFT Amp @75Hz	Amplitude (TKEO) [a.u.]	RMS (TKEO) [a.u.]
Displacement X [mm]	0.8863	0.0815	0.8865	0.0165	0.0010	0.0032	0.0026	0.0003
Displacement Y [mm]	1.1268	0.0922	1.1269	0.0131	0.0034	0.0081	0.0032	0.0004
Acceleration X [m/s²]	0.0044	2.2087	0.2447	0.0138	0.0560	0.0033	1.7265	0.1168
Acceleration Y [m/s²]	0.0058	2.5300	0.2851	0.0143	0.0296	0.0026	1.8172	0.1568

and 2.04 in Y, whereas RMS(Time) increased by 1.64 and 1.34. From Configuration A to C, the corresponding RMS(TKEO) ratios were 11.68 and 6.95, compared with 3.41 and 3.01 for RMS(Time). These numerical ratios must not be interpreted as a direct comparison of diagnostic sensitivity. Conventional RMS is linear with signal amplitude, whereas TKEO-derived quantities have a different, approximately quadratic amplitude scaling for harmonic components. The larger RMS(TKEO) ratios may therefore arise partly from the mathematical scaling of the operator and do not demonstrate better state separation or statistical superiority. The values are retained only as descriptive, within-indicator observations for this proof-of-concept dataset. The displacement RMS values require additional caution, because their non-zero means are close to the reported RMS values; consequently, they include a substantial static offset and cannot be interpreted as pure

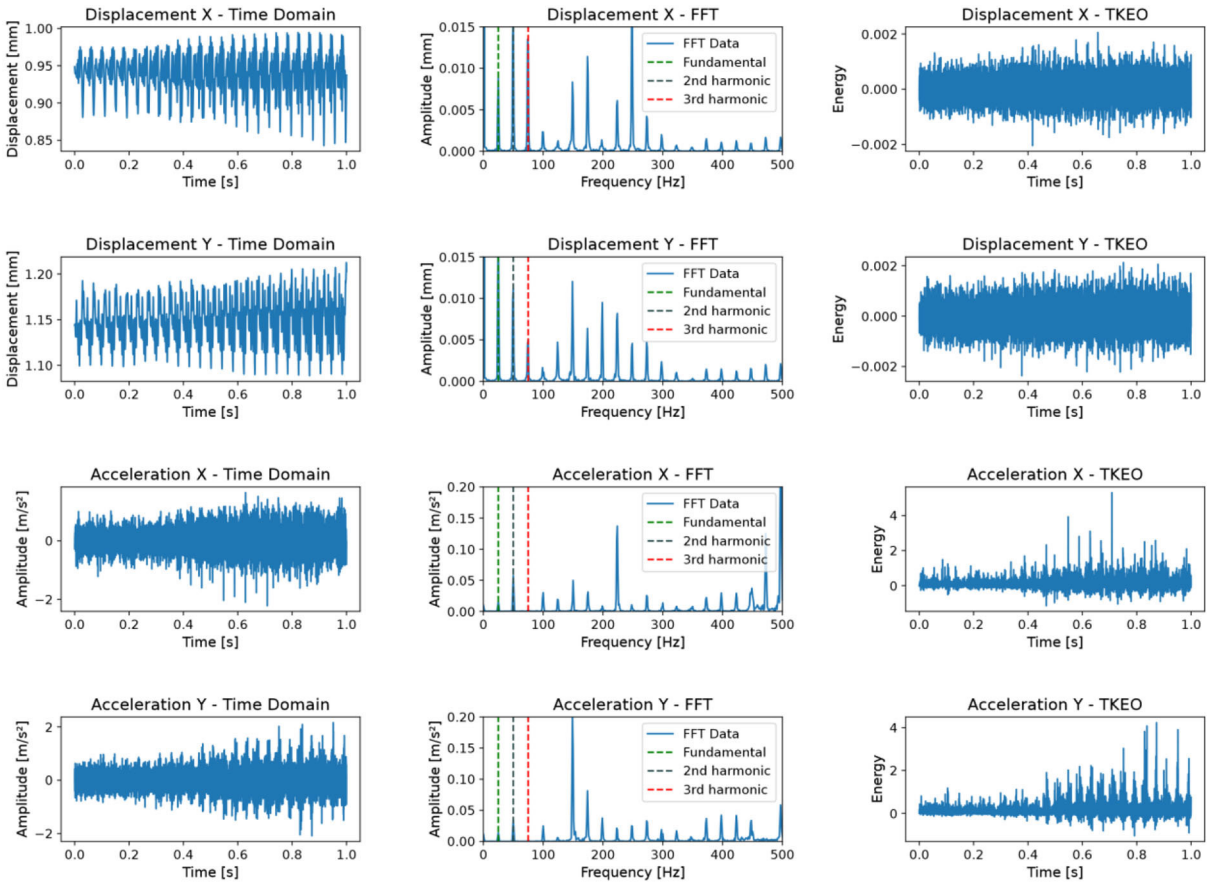


Figure 4. Vibration signal characteristics for the single retained record from the imposed bearing Configuration B, analysed using time-domain, FFT, and TKEO methods. Axis limits differ across panels and configurations and must be read from each displayed axis

Table 4. Descriptive parameters from the single retained displacement and acceleration record for the imposed bearing Configuration B

Channel	Mean (Time)	Amplitude (Time)	RMS (Time)	FFT Amp @25Hz	FFT Amp @50Hz	FFT Amp @75Hz	Amplitude (TKEO) [a.u.]	RMS (TKEO) [a.u.]
Displacement X [mm]	0.9381	0.1517	0.9385	0.00892	0.0143	0.0092	0.0041	0.0004
Displacement Y [mm]	1.1474	0.1239	1.1476	0.01792	0.0097	0.0049	0.0045	0.0005
Acceleration X [m/s²]	0.0042	3.8693	0.4022	0.0157	0.0579	0.0021	6.4597	0.2871
Acceleration Y [m/s²]	0.0057	4.2390	0.3832	0.0143	0.0341	0.0026	5.2787	0.3193

vibration-energy measures. Figure 6 presents the descriptive changes of the indicators across the three imposed configurations without implying a ranking of their diagnostic performance.

Figure 6 and Tables 3–5 summarise one retained representative record for each imposed bearing Configuration A–C. Four independent repeats were acquired for each analysed configuration, within a broader campaign of 175 measurements overall; however, the repeat-level values and raw records required to calculate dispersion measures or perform new inferential analyses were not available for this revision. The reported values are therefore descriptive only and cannot support error bars, confidence intervals, statistical significance tests, or claims of superiority or statistical diagnostic performance. They also do not independently identify the underlying physical states.

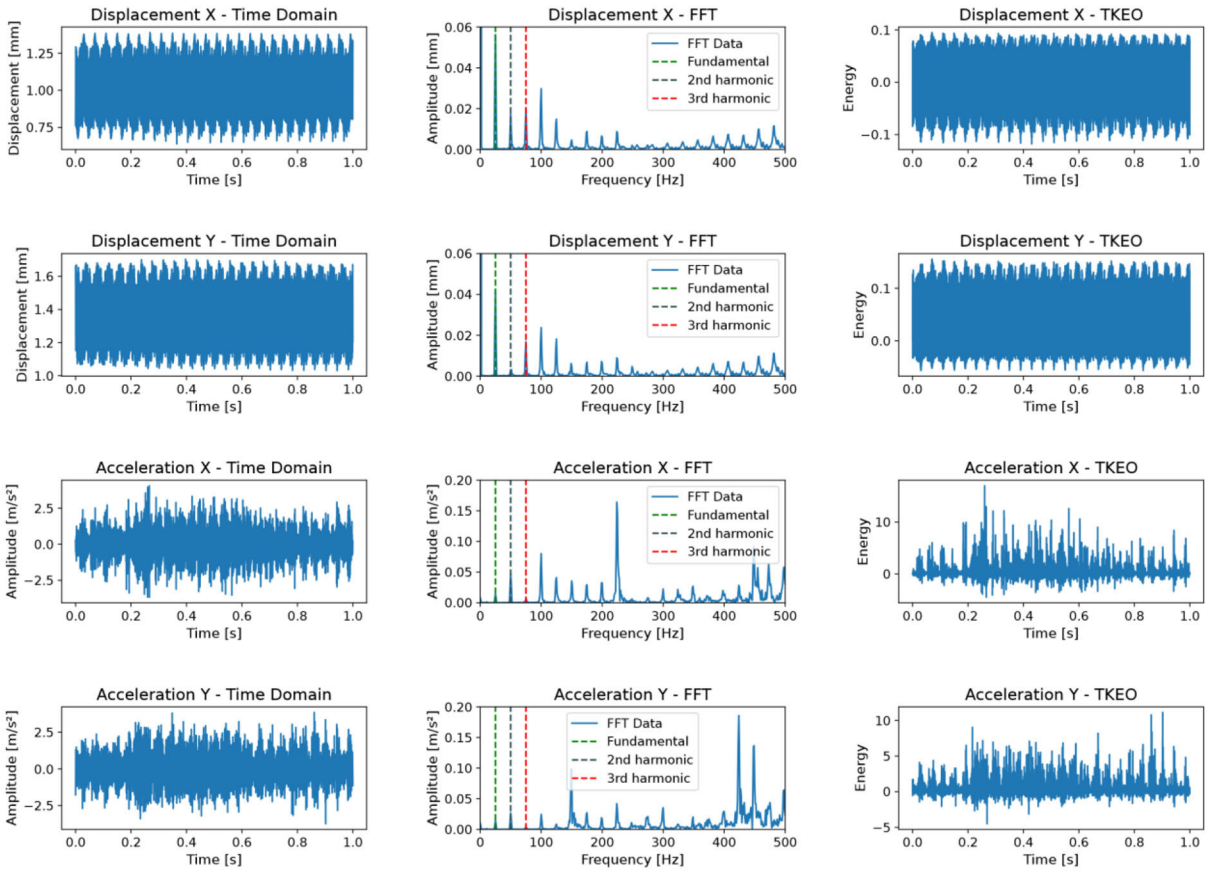


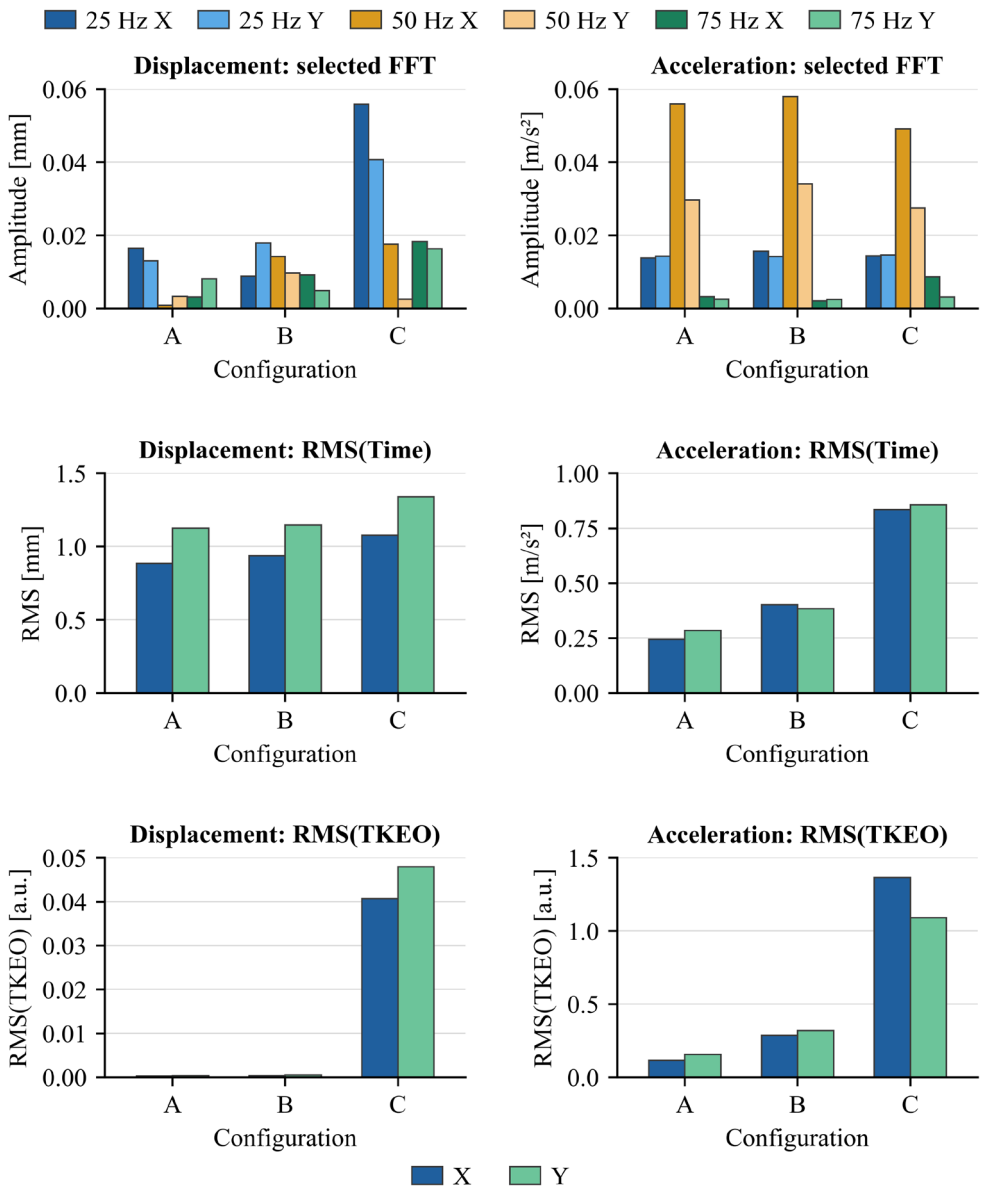
Figure 5. Vibration signal characteristics for the single retained record from the imposed bearing Configuration C, analysed using time-domain, FFT, and TKEO methods. Axis limits differ across panels and configurations and must be read from each displayed axis

Table 5. Descriptive parameters from the single retained displacement and acceleration record for the imposed bearing Configuration C

Channel	Mean (Time)	Amplitude (Time)	RMS (Time)	FFT Amp @25Hz	FFT Amp @50Hz	FFT Amp @75Hz	Amplitude (TKEO) [a.u.]	RMS (TKEO) [a.u.]
Displacement X [mm]	1.0626	0.7499	1.0788	0.055815	0.0176	0.0183	0.2126	0.0407
Displacement Y [mm]	1.3286	0.6731	1.3402	0.040713	0.0026	0.0163	0.2117	0.0479
Acceleration X [m/s²]	0.0039	7.7156	0.8352	0.014370	0.0491	0.0087	21.4695	1.3649
Acceleration Y [m/s²]	0.0049	7.5856	0.8571	0.014617	0.0275	0.0032	15.6231	1.0897

Table 6. Qualitative comparison of the roles, retained-record observations, and limitations of RMS, FFT, and TKEO

Method	Role in the present study	Observation from retained records	Main limitation
RMS	Overall time-domain magnitude	Values differed among Configurations A–C	Displacement RMS includes a static shaft-position component
FFT	Selected rotational and harmonic content	Components at 25, 50, and 75 Hz differed among retained records	Based on single representative records without dispersion analysis
TKEO	Local nonlinear signal-derived descriptor	TKEO amplitude and RMS(TKEO) differed among Configurations A–C	Noise- and bandwidth-sensitive; amplitude scaling differs from conventional RMS



Single retained record per configuration. Dispersion estimates are unavailable.

Figure 6. Descriptive comparison of displacement and acceleration responses across the single retained records for imposed bearing Configurations A–C. Axis ranges differ among panels and must be read from each displayed axis; the bars do not represent replicated measurements or uncertainty estimates

DISCUSSION

The simulated cases and experimental configurations were deliberately treated as two separate evidence streams. The simulations demonstrate how selected mathematical signal constructions affect the three processing domains. The experimental records show configuration-dependent differences on the test rig. No simulated case was mapped to Configuration A, B, or C, and the synthetic hydrodynamic-instability signal did not constitute evidence of hydrodynamic instability in the experiment.

The three analysis domains are complementary. Conventional RMS provides a compact measure of overall signal magnitude but loses temporal localisation. FFT reveals synchronous and harmonic components and is therefore useful for separating rotational content from broadband or impulsive behaviour. TKEO emphasises short-duration signal-derived changes, and its summary quantities differed among the retained configurations. Because TKEO-derived

quantities and conventional RMS have different amplitude scaling, their relative changes cannot be used to rank diagnostic sensitivity. The ratios reported here should nevertheless be interpreted as within-record contrasts, not as proof of statistical superiority. In addition, the displacement time-domain RMS values contain a substantial static component, so comparisons based only on those values would conflate shaft position with fluctuating vibration.

The operator's sensitivity is also its main practical weakness. Measurement noise, impulsive interference, and changes in bandwidth can produce large local energy values; recent bearing-diagnostic research likewise combines TKEO with additional signal-processing stages to obtain robust features [38]. The experimental records were low-pass filtered using a fourth-order Butterworth filter with a cutoff frequency of 100 Hz, without demeaning or detrending, and their FFT spectra were calculated from 1.0-s segments using a rectangular window with no additional taper. No amplitude-normalisation step is documented for the experimental TKEO calculation, and none is claimed. Absolute TKEO values from displacement and acceleration channels are not interpreted as directly comparable physical quantities. The non-zero displacement means remain in the reported RMS values, so displacement RMS includes a static-position component and is not interpreted as pure fluctuating vibration energy.

In contrast, the synthetic spectra in Figure 2 were generated using a Hann window and display the unscaled FFT magnitude calculated as np.abs(fft_signal), without amplitude normalisation. Therefore, the displayed synthetic FFT values cannot be interpreted as physical signal amplitudes in millimetres. No specific synthetic filtering step is claimed. Consequently, the results support TKEO as an additional indicator, rather than a stand-alone decision rule, and any threshold should be established from repeated measurements under known acquisition settings.

The water-lubricated bearing context is important because the measured response depends on clearance, material, groove configuration, water supply, and contamination, as well as on the nominal fault state. Vibration-based assessment has been investigated for water-lubricated bearings in other rotating systems and for additively manufactured bearing materials [39,40]. Wear tests further show that polymer material and groove layout affect the behaviour under contaminated-water lubrication [41]. These studies support the relevance of vibration monitoring but also caution against transferring a threshold between installations without accounting for bearing design and lubricant condition. In the present test, water was gravity-fed under an approximately 0.10 m hydrostatic head, while volumetric flow rate, supply pressure, and water temperature were not instrumentally measured. Therefore, the influence of hydrodynamic supply conditions cannot be quantified, and differences among Configurations A–C are interpreted descriptively, rather than attributed to a measured change in water-film conditions.

For centrifugal pumps, recent vibration-based classification studies demonstrate that richer representations can separate multiple fault classes under controlled conditions [42,43]. The present work addressed an earlier stage of that workflow: selection and interpretation of indicators. It did not report accuracy, sensitivity, specificity, or cross-validation. Its main limitations were the constant 25 Hz speed, one laboratory test rig, four repeats per analysed configuration without repeat-level results available for dispersion or inferential analysis, three imposed configurations without independent physical validation of their dynamic-state labels, incomplete clearance, groove-dimension, bearing-diameter, lubrication-supply metadata, and no underground field campaign. These limitations prevent claims of validated early-fault detection, statistical repeatability, or assignment of the configurations to confirmed hydrodynamic instability. They also define the evidence needed before deployment: preservation and analysis of repeat-level results, repeated tests over speed, load, clearance, and water-quality ranges, followed by field data and predefined classification metrics. Real-time implementation, multisensor fusion, and noise-robust preprocessing may then be evaluated without treating them as conclusions of the current proof-of-concept.

Taken together, the evidence supports a bounded conclusion: TKEO provides an additional local, nonlinear representation of the retained signals, while RMS and FFT retain complementary magnitude and frequency information. The study did not establish that any descriptor is superior. Its contribution is the transparent, application-specific comparison

Table 7. Relationship between the present proof-of-concept and earlier related studies by the authors

Study	Object/configuration	Lubrication/protocol	Signals/metrics	Scope relative to the present work
Blaut and Breńkacz [10]	Laboratory rotor supported by hydrodynamic plain bearings; balanced and deliberately unbalanced conditions.	Hydrodynamic-bearing laboratory system; multiple rotational speeds; the lubricant was not the application-specific distinction examined here.	Displacement, acceleration, and TKEO-based measures.	Established TKEO feasibility for rotor-unbalance assessment; it did not examine imposed Configurations A–C of the present water-lubricated proof-of-concept at a fixed 25 Hz.
Blaut [9]	Laboratory water-lubricated plain-bearing records, including shaft displacement and rotational trajectories.	Grooved bearing with closed water circulation; signal segments described in that study as unstable, transitional, and stable at constant speed.	Dispersion entropy and trajectory-based interpretation of X and Y displacement.	Examined DisEn on a related water-lubricated bearing system. The present study uses Configuration A–C terminology and does not adopt the earlier labels as independent physical validation.
Blaut and Breńkacz [8]	Synthetic, nonlinear-system, and real bearing-displacement signals analysed in sliding windows.	Bearing configuration and lubricant were not the principal comparison; the protocol focused on window length.	Sliding-window dispersion entropy and stability of the result with window length.	Addressed the window-length dependence of DisEn rather than the combined RMS–FFT–TKEO description used here.
Present study	Four illustrative synthetic signals and retained displacement and acceleration records for imposed Configurations A–C.	Water-lubricated plain bearing; fixed 25 Hz shaft speed; configurations imposed by rotating the bearing and changing the lubrication gap location.	Mean, amplitude, RMS, FFT amplitudes at 25, 50, and 75 Hz, TKEO amplitude, and RMS(TKEO).	Provides an application-specific descriptive comparison. The simulations illustrate method response and do not validate or map one-to-one onto Configurations A–C.

of these representations under a single controlled laboratory protocol.

Relation to earlier studies and specific contribution

The present study built on earlier work, but addressed a narrower application-specific question. Previous studies examined TKEO for rotor-unbalance assessment in hydrodynamic bearings [10], dispersion entropy for characterisation of water-lubricated bearing records [9], and the effect of sliding-window length on dispersion-entropy analysis [8]. The present contribution is not a new bearing-state validation or a first demonstration of either TKEO or the test rig. It combined conventional RMS, selected FFT components, and TKEO-derived descriptors for both displacement and acceleration records from imposed Configurations A–C and places these experimental observations alongside separate synthetic illustrations. Table 7 summarises these distinctions. No new tribological or lubrication-film phenomenon was independently measured or validated; the configuration labels therefore denote imposed test conditions, rather than confirmed lubrication-film states.

CONCLUSIONS

This laboratory proof-of-concept evaluated the Teager-Kaiser energy operator for a water-lubricated plain-bearing pump using four synthetic signal cases and three imposed bearing configurations (A–C). The four synthetic cases served only as illustrations of method response and were not used to validate, classify, or assign physical meanings to experimental Configurations A–C. The specific contribution is the descriptive application of a common RMS–FFT–TKEO framework to displacement and acceleration records from a water-lubricated plain bearing, not the validation of a new diagnostic-state model. The configurations were produced by changing the bearing orientation and lubrication-gap location and were not independently validated as stable, transient, or unstable dynamic states. The simulations showed distinct TKEO responses for harmonic, unbalance-related, impulsive, and noise-modulated inputs, while both conventional and TKEO-derived indicators changed across the experimental records. The numerical configuration-to-configuration ratios of RMS(Time) and RMS(TKEO) are not directly comparable, because the indicators have different amplitude scaling. Consequently, the present

results did not demonstrate that TKEO has greater diagnostic sensitivity or statistical superiority over conventional RMS.

Within this scope, TKEO should be treated as a complementary signal representation rather than a replacement for conventional diagnostics. RMS summarises overall signal magnitude, FFT retains rotational and harmonic information, and TKEO emphasises rapid joint changes in amplitude and frequency. The observations describe configuration-dependent differences only and do not establish physical-state labels, hydrodynamic instability, or a diagnostic fault mechanism. Displacement RMS requires cautious interpretation because no demeaning or detrending was applied, and the reported values include a substantial mean component. Although four independent repeats were acquired for each analysed configuration, only retained representative results were available for the present tables and figures; repeat-level dispersion and statistical repeatability were not established. The findings are limited to a single rig at a constant 25 Hz speed and do not establish classification accuracy or field performance. The absence of measured volumetric flow rate, supply pressure, and instrumentally recorded water temperature further limits transferability; the present results do not establish how controlled lubrication-supply parameters affect the observed configuration-dependent responses.

Acknowledgements

Calculations were carried out at the Academic Computer Center in Gdańsk.

This research was funded by the National Centre for Research and Development (NCBR), LIDER programme, project no. LIDER15/0168/2024.

Data availability

The retained representative records and recovered simulation materials used for the analyses reported in this article are available from the corresponding author upon reasonable request. Repeat-level raw records from the broader experimental campaign were not available for the present revision and are not represented in the reported tables or figures.

REFERENCES

1. Zhou J., Di L., Cheng C., Xu Y., Lin Z. A rotor unbalance response based approach to the identification of the closed-loop stiffness and damping coefficients of active magnetic bearings. Mechanical Systems and Signal Processing. 2016; 66–67: 665–678. https://doi.org/10.1016/j.ymssp.2015.06.008
2. Čudina M., Prezelj J. Detection of cavitation in operation of kinetic pumps. Use of discrete frequency tone in audible spectra. Applied Acoustics. 2009; 70(4): 540–546. https://doi.org/10.1016/j.apacoust.2008.07.005
3. Riedemann J., Reyes E., Sarasiri N., Pena R., Andrade I. Renewable source-based water pumping electrification in mines: current technologies and future trends. IEEE Electrification Magazine. 2024; 12(1): 38–44. https://doi.org/10.1109/MELE.2023.3348349
4. Sottile J., Holloway L.E. An overview of fault monitoring and diagnosis in mining equipment. IEEE Transactions on Industry Applications. 1994; 30(5): 1326–1332. https://doi.org/10.1109/28.315247
5. Kleinmann S., Kościelny J.M., Koller-Hodac A., Paczynski A., Stetter R. Concept of an advanced monitoring, control and diagnosis system for positive displacement pumps. In: 2010 Conference on Control and Fault-Tolerant Systems (SysTol). IEEE; 2010. p. 233–238. https://doi.org/10.1109/SYSTOL.2010.5676057
6. Andrearczyk A., Żywica G., Breńkacz Ł., Bagiński P. Vibration based diagnostics of the multi-stage microturbine operating in the medium-temperature ORC system. Vibroengineering Procedia. 2017; 13: 56–61. https://doi.org/10.21595/vp.2017.19024
7. Drosińska-Komor M., Głuch J., Breńkacz Ł., Ziółkowska N., Piotrowicz M., Ziółkowski P. Advanced genetic algorithm-based signal processing for multi-degradation detection in steam turbines. Mechanical Systems and Signal Processing. 2025; 224: 112166. https://doi.org/10.1016/j.ymssp.2024.112166
8. Blaut J., Breńkacz Ł. Application of the dispersion entropy with sliding window for the analysis of mechanical systems. Diagnostyka. 2024; 25(4): 1–12. https://doi.org/10.29354/diag/195473
9. Blaut J. Application of dispersion entropy to journal bearing hydrodynamic stability. Vibrations in Physical Systems. 2024; 35(2): 2024217. https://doi.org/10.21008/j.0860-6897.2024.2.17
10. Blaut J., Breńkacz Ł. Application of the Teager-Kaiser energy operator in diagnostics of a hydrodynamic bearing. Eksploatacja i Niezawodność - Maintenance and Reliability. 2020; 22(4): 757–765. https://doi.org/10.17531/ein.2020.4.20

11. Mazur D.C., Kay J.A., Mazur K.D. Advancements in vibration monitoring for the mining industry. In: 2014 IEEE Industry Application Society Annual Meeting. IEEE; 2014. p. 1–8. https://doi.org/10.1109/IAS.2014.6978459
12. Al-Braik A., Hamomd O., Gu F., Ball A.D. Diagnosis of impeller faults in a centrifugal pump using vibration signals. In: Eleventh International Conference on Condition Monitoring and Machinery Failure Prevention Technologies; 10-12 June 2014; Manchester, UK. British Institute of Non-Destructive Testing; 2014. p. 603–612. Available from: https://eprints.hud.ac.uk/id/eprint/21052/
13. Moczulski W., Przystałka P., Sikora M., Zimroz R. Modern ICT and mechatronic systems in contemporary mining industry. In: Rough Sets. Lecture Notes in Computer Science. Springer International Publishing; 2016. p. 33–42. https://doi.org/10.1007/978-3-319-47160-0_3
14. Stankiewicz K., Jasiulek D., Rogala-Rojek J., Bartoszek S. Selected, state-of-the-art mechatronic systems in Polish underground mining industry. In: Proceedings of the 30th International Symposium on Automation and Robotics in Construction and Mining (ISARC 2013). International Association for Automation and Robotics in Construction; 2013. p. 119–129. https://doi.org/10.22260/ISARC2013/0013
15. Sánchez F., Hartlieb P. Innovation in the mining industry: technological trends and a case study of the challenges of disruptive innovation. Mining, Metallurgy & Exploration. 2020; 37(5): 1385–1399. https://doi.org/10.1007/s42461-020-00262-1
16. Zhang X.L., Yin Z.W., Jiang D., Gao G.Y. Comparison of the lubrication performances of water-lubricated and oil-lubricated plain journal bearings. Applied Mechanics and Materials. 2014; 711: 27–30. https://doi.org/10.4028/www.scientific.net/AMM.711.27
17. Korotkov A., Korotkova L., Vidin D. Study of the quality of plain bearings used in mining machinery. E3S Web of Conferences. 2023; 402: 10029. https://doi.org/10.1051/e3sconf/202340210029
18. Rea I., Monaghan D. Dewatering bore pumps - reducing costs and emissions by maximising pumping efficiency over time. Mining Technology. 2009; 118(3–4): 220-224. https://doi.org/10.1179/174328610X12682159815109
19. Breńkacz Ł., Żywica G., Drosińska-Komor M. The experimental identification of the dynamic coefficients of two hydrodynamic journal bearings operating at constant rotational speed and under nonlinear conditions. Polish Maritime Research. 2017; 24(4): 108–115. https://doi.org/10.1515/pomr-2017-0142
20. Breńkacz Ł., Żywica G., Drosińska-Komor M., Szewczuk-Krypa N. The experimental determination of bearings dynamic coefficients in a wide range of rotational speeds, taking into account the resonance and hydrodynamic instability. In: Dynamical Systems in Applications. Springer Proceedings in Mathematics & Statistics. Springer International Publishing; 2018. p. 13–24. https://doi.org/10.1007/978-3-319-96601-4_2
21. Beck D., Wulff S., Thamsen P.U., Reich M., Worringer J.P. Recommendations for long-term operation of high-performance submersible motor pumps in mine dewatering. In: ASME 2020 Fluids Engineering Division Summer Meeting. Volume 1: Fluid Applications and Systems; Fluid Measurement and Instrumentation. American Society of Mechanical Engineers; 2020. Article V001T01A015. https://doi.org/10.1115/FEDSM2020-20245
22. Zotov V.V., Mnatsakanyan V.U., Bazlin M.M., Lakshinsky V.S., Dyatlova E.V. Extending the service life of centrifugal dewatering pump impellers in mines. Mining Industry Journal (Gornaya Promyshlennost). 2024; (2): 143–146. https://doi.org/10.30686/1609-9192-2024-2-143-146
23. Noon A.A., Kim M.H. Erosion wear on centrifugal pump casing due to slurry flow. Wear. 2016; 364–365: 103–111. https://doi.org/10.1016/j.wear.2016.07.005
24. Peng G.J., Luo Y.Y., Wang Z.W. Research on wear properties of centrifugal dredge pump based on liquid-solid two-phase fluid simulations. IOP Conference Series: Materials Science and Engineering. 2015; 72(4): 042048. https://doi.org/10.1088/1757-899X/72/4/042048
25. Lai F., Zhu X., Xu X., Li G. Erosion wear and performance simulation of centrifugal pump for solid-liquid flow. In: ASME 2018 Power Conference. Volume 2: Heat Exchanger Technologies; Plant Performance; Thermal Hydraulics and Computational Fluid Dynamics; Water Management for Power Systems; Student Competition. American Society of Mechanical Engineers; 2018. Article V002T10A001. https://doi.org/10.1115/POWER2018-7151
26. Shen Z., Chu W. Effect of particle parameters on erosion wear and performance of screw centrifugal pump. In: ASME 2018 International Mechanical Engineering Congress and Exposition. Volume 7: Fluids Engineering. American Society of Mechanical Engineers; 2018. Article V007T09A018. https://doi.org/10.1115/IMECE2018-88586
27. Tarodiya R., Gandhi B.K. Experimental investigation of centrifugal slurry pump casing wear handling solid-liquid mixtures. Wear. 2019; 434–435: 202972. https://doi.org/10.1016/j.wear.2019.202972
28. Llewellyn R.J., Yick S.K., Dolman K.F. Scouring erosion resistance of metallic materials used in slurry pump service. Wear. 2004; 256(6): 592–599. https://doi.org/10.1016/j.wear.2003.10.002

29. Singh J., Singh S. Neural network prediction of slurry erosion of heavy-duty pump impeller/casing materials 18Cr-8Ni, 16Cr-10Ni-2Mo, super duplex 24Cr-6Ni-3Mo-N, and grey cast iron. Wear. 2021; 476: 203741. https://doi.org/10.1016/j.wear.2021.203741
30. Xie Y., Jiang J., Islam M.A. Elastomers and plastics for resisting erosion attack of abrasive/erosive slurries. Wear. 2019; 426–427: 612–619. https://doi.org/10.1016/j.wear.2019.01.123
31. Stawarz M., Dojka M. Corrosion resistance of selected cast iron grades under deposit mining conditions. International Journal of Metalcasting. 2022; 16(1): 342–348. https://doi.org/10.1007/s40962-021-00607-6
32. Ovchinnikov N.P. Establishing the causes for low operational reliability of slurry pumps based on a system analysis. Obogashchenie Rud. 2020; (5): 41–46. https://doi.org/10.17580/or.2020.05.07
33. Zhu D.C., Zhang Y.X., Zhu Q.W. Fault diagnosis method for rolling element bearings under variable speed based on TKEO and Fast-SC. Journal of Failure Analysis and Prevention. 2018; 18(1): 2–7. https://doi.org/10.1007/s11668-018-0383-y
34. Guo K., Ma J., Xiong X., Hu Y., Li X. Fault feature extraction method of rolling bearing based on IAFD and TKEO. Journal of Sensors. 2024; 2024: 8551009. https://doi.org/10.1155/2024/8551009
35. Solnik S., Rider P., Steinweg K., DeVita P., Hortobágyi T. Teager-Kaiser energy operator signal conditioning improves EMG onset detection. European Journal of Applied Physiology. 2010; 110(3): 489–498. https://doi.org/10.1007/s00421-010-1521-8
36. Xu Y., Zhou J., Lin Z., Jin C. Identification of dynamic parameters of active magnetic bearings in a flexible rotor system considering residual unbalances. Mechatronics. 2018; 49: 46–55. https://doi.org/10.1016/j.mechatronics.2017.11.004
37. Breńkacz Ł., Rumin R., Blaut J. Method for precision automatic unbalance control in wind turbines by continuously adjusting correction mass. Advances in Science and Technology Research Journal. 2026; 20(2): 212–242. https://doi.org/10.12913/22998624/210041
38. Shi X., Zhang Z., Xia Z., Li B., Gu X., Shi T. Application of Teager-Kaiser energy operator in the early fault diagnosis of rolling bearings. Sensors. 2022; 22(17): 6673. https://doi.org/10.3390/s22176673
39. Matania O., Heletz S., Klein R., Groper M., Bortman J. Toward diagnostics of water-lubricated bearings of naval vessels by vibration analysis. Structural Health Monitoring. 2023; 22(4): 2565–2578. https://doi.org/10.1177/14759217221125064
40. Blaut J. Assessment of the impact of 3D printed water-lubricated cutless bearings material on vibration parameters. Decision Making in Manufacturing and Services. 2022; 16: 5–17. https://doi.org/10.7494/dmms.2022.16.5980
41. Litwin W., Wasilczuk M., Wodtke M., Olszewski A. The influence of polymer bearing material and lubricating grooves layout on wear of journal bearings lubricated with contaminated water. Tribology International. 2023; 179: 108159. https://doi.org/10.1016/j.triboint.2022.108159
42. Zaman W., Ahmad Z., Siddique M.F., Ullah N., Kim J.M. Centrifugal pump fault diagnosis based on a novel SobelEdge scalogram and CNN. Sensors. 2023; 23(11): 5255. https://doi.org/10.3390/s23115255
43. Gonçalves J.P.S., Fruett F., Dalfré Filho J.G., Giesbrecht M. Faults detection and classification in a centrifugal pump from vibration data using Markov parameters. Mechanical Systems and Signal Processing. 2021; 158: 107694. https://doi.org/10.1016/j.ymssp.2021.107694